P3-31

Details of neutral transport in gas puff imaging experiments

D.P. Stotler [a,*], J. Boedo [b], B. LeBlanc [a], R.J. Maqueda [c], and S. J. Zweben [a]

[a] *Princeton Plasma Physics Laboratory, Princeton University, P. O. Box 451, Princeton, NJ 08543-0451, USA*

[b] *University of California at San Diego, San Diego, CA, USA*

[c] *Nova Photonics, Los Alamos, NM, USA*

Abstract

Gas puff imaging (GPI) experiments are designed to provide high time and space resolution data on the structure of plasma turbulence in the plane perpendicular to the magnetic field. We first examine the temporal behavior of the helium atoms used as the emitting species for GPI and show that for the time scales of interest ($\gtrsim 1$ μs), the atomic physics model underlying the conventional interpretation of GPI is valid. Second, we continue the Monte Carlo neutral transport simulations of the GPI diagnostic begun in [1]. The radial characteristics of the simulated emission clouds match observations to within the estimated errors. The upshot of these two

results is that the technique for unfolding the 2-D, time-dependent plasma density and temperature data from helium GPI emission, relying on this atomic physics

model and utilizing DEGAS 2's simulated neutral density data, is valid.

Key words: (PSI-17) Neutral modeling, DEGAS, NSTX, Edge plasma, Collisional-radiative model, (JNM) T0100 Theory and Modeling

PACS: 52.25.Ya, 52.55.Fa, 52.65.Pp, 52.70.Kz

---

1 Introduction

The gas puff imaging (GPI) diagnostic [2,3,4] is designed to provide high time resolution, two-dimensional (2-D) data on plasma turbulence for comparison with three-dimensional (3-D) nonlinear plasma simulation codes, reduced theoretical turbulence models, and direct probe measurements of the turbulence. The technique consists of recording with high temporal and spatial resolution [2] light generated by neutral atoms puffed into the edge of the plasma.

Previous modeling and analysis [3,5] have demonstrated that the behavior of the neutral atoms does not cause the spatial characteristics of the observed emission patterns to deviate qualitatively from those of the underlying plasma turbulence. In Sec. 2, we will examine the impact of the atoms on the temporal characteristics of the GPI diagnostic, using the methods of [6] to show for the time scales of

* Corresponding and presenting author
Email address: dstotler@pppl.gov (D.P. Stotler).

interest that the model behind the conventional interpretation of GPI data is valid. In Sec. 3, we continue the comparison of 3-D, steady state DEGAS 2 [7] neutral transport simulations with GPI observations, begun in [1], using data from 2004 NSTX experiments [4].

2 Time Dependent Response of Helium Atomic Physics Models

2.1 Criteria for Evaluating Collisional Radiative Models

The conventional interpretation of GPI [3] relies on an atomic physics model in which only the atom's ground state is explicitly considered; the effects of all excited states are folded into effective rates for ionization and photon emission. This approach assumes first that this approximate atomic physics model is valid for the parameters of interest and second that the time response of this model for GPI-relevant plasma density and temperature changes is accurate. However, these assumptions may not always be true, particularly when metastable states, such as the 2^1S and 2^3S states in helium, are involved. If these assumptions are violated, the temporal *and spatial* characteristics of the observed turbulence could differ from those of the underlying plasma turbulence. A more complex helium atomic physics model requiring the explicit consideration of these metastable states in addition to the ground state is also available [8,9]. The same questions of validity

and time response can be asked of this model. Furthermore, one would like to know if the added complexity of this model is offset by a wider range of validity or by better time resolution.

The full system of equations describing the evolution of the various helium atomic states can be written as [6,8,9,10]

$$\dot{\mathbf{n}} = \mathbf{M}\mathbf{n} + \mathbf{\Gamma}, \tag{1}$$

where $\mathbf{n}$ is a vector of N atomic states, 1^1S, 2^1S, 2^3S, 2^1P, 2^3P, 3^1S, etc., $\mathbf{M}$ is an $N \times N$ matrix of rates, and $\mathbf{\Gamma}$ represents sources of the states. Since the detailed contributions to $\mathbf{M}$ are not referred to further in this paper, we will only note that they consist of the rates for collisional ionization, excitation, de-excitation, radiative decay, and recombination (three body, radiative, and dielectronic). The reader should refer to [9] for additional details on these rates.

The general tactic behind the effective atomic physics models we consider here, referred to as "collisional radiative" (CR) models, [11,12] is to first divide the N states into two sets P and Q (following Greenland's nomenclature [6,10]):

$$\begin{bmatrix} \dot{\mathbf{n}}_P \\ \\ \dot{\mathbf{n}}_Q \end{bmatrix} = \begin{bmatrix} \mathbf{M}_P & \mathbf{H} \\ \\ \mathbf{V} & \mathbf{M}_Q \end{bmatrix} \begin{bmatrix} \mathbf{n}_P \\ \\ \mathbf{n}_Q \end{bmatrix} + \begin{bmatrix} \mathbf{\Gamma}_P \\ \\ \mathbf{\Gamma}_Q \end{bmatrix}, \tag{2}$$

where there are N_P states in the set P and N_Q in Q, with $N = N_P + N_Q$. Then,

the behavior of the Q states is folded into a set of effective rates, $\mathbf{M}_{\rm eff}$ so that the full system can be described approximately by

$$\dot{\mathbf{n}}_P = \mathbf{M}_{\rm eff}\mathbf{n}_P + \mathbf{\Gamma}'_P. \tag{3}$$

A set of population coefficients provides the densities of the Q states in terms of the $\mathbf{n}_P$,

$$\mathbf{n}_Q = \mathbf{\Omega}\mathbf{n}_P - \mathbf{M}_Q^{-1}\mathbf{\Gamma}_Q. \tag{4}$$

Since N_P is typically on the order of a few and much smaller than N (e.g., 59 for helium [9]), the advantages of this approximate representation are clear. The papers by Greenland[6,10] provide specific criteria for assessing the validity of a particular choice for the P and Q states and give the timescales for which Eqs. (3) and (4) accurately describes the evolution of the full equations, Eq. (1). Greenland actually provides an algorithm for choosing the P and Q states, although we do not apply it here.

Greenland's criteria utilize the normalized eigenvectors and eigenvalues of $\mathbf{M}$. The N eigenvectors are used as the columns of an $N \times N$ matrix $\mathbf{T}$, arranged in order of increasing eigenvalue, $\lambda^{(i)}$, $i = 1, \ldots, N$. The resulting matrix is then broken up

into four sub-matrices as in Eq. (2),

$$\mathbf{T} = \begin{bmatrix} \mathbf{T}_P & \boldsymbol{\Delta} \\ \boldsymbol{\delta} & \mathbf{T}_Q \end{bmatrix}. \tag{5}$$

Greenland shows that in order for a particular CR model to be valid (i.e., a particular choice of the sets P and Q), one must have $\|\boldsymbol{\delta}\| \ll 1$ and $\|\mathbf{T}_Q^{-1}\boldsymbol{\delta}\| \ll 1$ [6]. Furthermore, if the largest P space eigenvalue is much less than the smallest Q space eigenvalue, $|\lambda_P| \ll |\lambda_Q|$, then the usual prescription (e.g., as in [11,12]) for determining $\mathbf{M}_{\text{eff}}$ and $\boldsymbol{\Omega}$ applies [6]. The time scales corresponding to the inverses of these eigenvalues characterize the time resolution provided by the CR model. In particular, phenomena occurring faster than $\tau_Q \equiv 1/|\lambda_Q|$ are not resolved; i.e., the model treats those time scales as being instantaneous.

2.2 Application to Helium Collisional Radiative Models

Following [8] and [9], we consider two collisional radiative models for helium. In "Formulation I", the P states consist of the ground state 1^1S and the two metastable $n = 2$ states, 2^1S, and 2^3S ($N_P = 3$). In "Formulation II", the set P contains just the ground state ($N_P = 1$). We will use two sets of plasma parameters relevant to NSTX GPI experiments [3,4]. One ($T_e = 3$ eV, $n_e = 10^{18}$ m^{-3}) represents the far SOL near the gas manifold; the second ($T_e = 15$ eV, $n_e = 6 \times 10^{18}$

m^{-3}) is characteristic of the center of the emission cloud. We also consider a third low density set of parameters ($T_e = 30$ eV, $n_e = 10^{16}$ m^{-3}), typical of those used in the original work of Fujimoto [8].

The results of applying the analysis described in [6] and Sec. 2.1 to Goto's CR models [9] are presented in Table 1. The $N_P = 1$ CR model yields $\|\boldsymbol{\delta}\| \ll 1$ and $\|\mathbf{T}_Q^{-1}\boldsymbol{\delta}\| \ll 1$ in all three cases, and is, thus, valid for these plasma conditions, albeit with varying time resolution, τ_Q. The $N_P = 3$ model, however, has small $\|\boldsymbol{\delta}\|$ and $\|\mathbf{T}_Q^{-1}\boldsymbol{\delta}\|$ only in the lowest density case; its validity for the "far SOL" parameters may be marginal. For the "cloud center" conditions, it is not valid at all!

To confirm these conclusions and to gain quantitative insight into the time resolution of the CR model, we next consider direct integration of Eqs. (1), (3) and (4). In particular, we assume an initial 1^1S density of unity and steady plasma parameters. The 3^3D state (upper state for the 587.6 nm line used in the GPI experiments) densities obtained for the GPI relevant density and temperature pairs are depicted in Fig. 1. The τ_Q values from Table 1 are included in Fig. 1 to facilitate comparison with the above analysis.

The validity of the $N_P = 1$ CR model for both plasma parameter sets at times later than τ_Q is confirmed by the convergence of its 3^3D density with that from

$(T_e$ eV, n_e m$^{-3}) =$	$(3,\ 10^{18})$	$(15,\ 6\times10^{18})$	$(30,\ 10^{16})$
$N_P = 1$: $\|\boldsymbol{\delta}\|$	8.2×10^{-5}	2.5×10^{-3}	1.0×10^{-2}
$\|\mathbf{T}_Q^{-1}\boldsymbol{\delta}\|$	8.7×10^{-5}	1.9×10^{-3}	1.0×10^{-2}
τ_Q (μs)	14	0.61	980
$N_P = 3$: $\|\boldsymbol{\delta}\|$	7.3×10^{-2}	5.4×10^{-1}	1.6×10^{-3}
$\|\mathbf{T}_Q^{-1}\boldsymbol{\delta}\|$	1.1×10^{-1}	6.9×10^{-1}	2.7×10^{-3}
τ_Q (μs)	0.087	0.045	0.52

Table 1

The results of applying Greenland's validity criteria [6] to the helium collisional radiative models described by [9].

the full equations. For the $T_e = 3$ eV, $n_e = 10^{18}$ m^{-3} case, the $N_P = 3$ CR model exhibits similar behavior. Under these conditions, the $N_P = 3$ model could be used to obtain higher time resolution than that provided by the $N_P = 1$ CR model. However, for the "cloud center" parameters, the $N_P = 3$ density does not converge to that of the full equations until the τ_Q of the $N_P = 1$ model is reached. This is a consequence of the $N_P = 3$ model being invalid at these parameters.

We conclude that the $N_P = 1$ CR model is valid for the parameters of interest and provides the $\sim \mu$s time resolution needed for the GPI diagnostic at "cloud center"

conditions. Note that emission in the far SOL is negligible so that the model's slower time response there is not relevant. This conclusion has been further confirmed with additional time-dependent integrations utilizing time varying plasma parameters typical of GPI observations in NSTX. The evolution of the 3^3D density obtained with the $N_P = 1$ model closely tracks that found with the full equations. Even when the plasma parameters change on time scales shorter than τ_Q, the time varying photon emission computed from the model is still qualitatively similar to that obtained from the full equations, although the quantitative details such as blob shape, size, and amplitude could differ in this case.

3 Three-Dimensional Modeling

We now turn to the 3-D DEGAS 2 simulations of NSTX GPI experiments, which utilize this $N_P = 1$ CR model for helium [9]. As in [5], these simulations are fully 3-D, including the shape of the gas manifold and emulation of the 64 by 64 pixel fast camera view. The resulting (steady state) 587.6 nm camera images are again compared with the median average [5] over the 300 frames recorded by the GPI camera. We use the median, rather than simple, average so as to minimize the effect of "blobs", yielding an emission cloud representative of the quiescent background plasma. The nonlinearity in the GPI camera response [4] has been fit with a power law function (exponent of 0.475), and the inverse of that function applied to the

GPI data so that the resulting quantity is proportional to the number of photons / m^2 s st striking the camera lens.

We consider here NSTX discharges 112811 (H-mode) and 112814 (L-mode). The DEGAS 2 meshes are based on EFIT equilibria at the times of interest. The plasma densities and temperatures are derived from Thomson scattering profiles taken at midplane and are assumed to be constant on a flux surface with $n_i = n_e$ and $T_i = T_e$. For shot 112814, the smoothed Thomson profiles taken at $t = 0.277$ s and 0.293 s have been averaged to approximate the profiles at the time of the GPI observation, $t = 0.285$ s (Fig. 2). Note that the camera used in these experiments differs from that referred to in [5] and that the geometric calibrations required as input to DEGAS 2 have been carefully executed and repeated multiple times during the NSTX campaign to catch any unintended changes to the configuration.

The camera images from the resulting simulations are shown in Fig. 3. The color map has been adjusted so that the cyan contour roughly corresponds to half of the peak value. The 25%, 50%, and 75% contours from the median average of the GPI data are overlaid on these images. As indicated by the arrows in Fig. 3, the GPI camera is oriented [4] so that the horizontal axis of its field of view is locally perpendicular to flux surfaces and its vertical axis is aligned with the flux surfaces. The camera's field of view corresponds to a 20 cm by 20 cm square about 20 cm above midplane and roughly centered on the separatrix. The core plasma is to the

left of the frame and the gas manifold is at its right edge.

The simulated and experimental images are well aligned; the misalignment of the images noted in [5] was likely due to a problem with the geometric calibration of the camera. For the H-mode shot 112811, the radial FWHM of the GPI emission cloud is 3 cm, compared with 2 cm in the simulation. For the L-mode shot 112814, the observed and simulated FWHM are both about 4 cm. In both simulations, the emission cloud is $\sim$ 2 cm farther in radially than the observed cloud. Given that the spatial resolution of the GPI diagnostic is 1–2 cm [4] and that the radial location of the Thomson scattering points is uncertain to within $\sim$ 1 cm (Fig. 2), the radial characteristics of the baseline and the observed emission clouds are in good agreement.

The poloidal extent of the simulated emission clouds is greater than that seen in the GPI images. In fact, the half-peak contours for these simulations extend outside the camera frame. One possible explanation for this apparent discrepancy is that the vertical extent of the experimental image is limited by vignetting of the camera lens. Another is that the gas flow out of the holes in the manifold is not uniform along its length, as is assumed in the simulations.

4 Conclusions

The analysis of Sec. 2 leads us to conclude that the single state atomic physics model conventionally used in the interpretation of helium GPI experiments is valid for the relevant range of plasma parameters and provides adequate time resolution at the cloud center. We are then justified in exploiting the simple relationship between the plasma parameters and the GPI light emission, S, provided by this model: $S = n_0 F(n_e, T_e)$, where F represents the photon emission rate per atom computed from the model. If the neutral density n_0 appearing in this relation can be estimated, the spatial and temporal variation of the plasma parameters can be unfolded from the GPI images [1] by inverting F. The resulting 2-D and time-varying data can then be used, for example, to test models of blob birth and propagation [13]. The 3-D, steady state DEGAS 2 neutral transport simulations described in Sec. 3 give the neutral density required by this technique. The fidelity of this neutral density profile, and indeed, of the entire model of the helium-based GPI diagnostic, is confirmed by the satisfactory agreement between the simulated and observed emission clouds noted in that section.

These comparisons effectively ignore the impact of blobs on the light emission through the use of the single time Thomson scattering profiles and the median average of the GPI data. Because the relation between the plasma parameters and

the light emission is nonlinear, there is no obvious method for incorporating the blobs in an average fashion. Instead, they would likely have to be dealt with via time-dependent and 3-D plasma profiles.

Acknowledgments

This work supported by U.S. DOE Contracts DE-AC02-76CHO3073, DE-FG03-95ER54294, and DE-FG02-04ER54520. The authors would like to thank S. A. Sabbagh for generating EFIT equilibria for 112811 on short notice.

References

[1] D. P. Stotler et al., Contrib. Plasma Phys. 44 (2004) 294.

[2] R. J. Maqueda et al., Sci. Instrum. 74 (2002) 2020.

[3] S. J. Zweben et al., Nucl. Fusion 44 (2004) 134.

[4] S. J. Zweben et al., Phys. Plasmas 13 (2006) 056114.

[5] D. P. Stotler et al., J. Nucl. Mater. 313–316 (2003) 1066.

[6] P. T. Greenland, J. Nucl. Mater. 290–293 (2001) 615.

[7] D. P. Stotler, C. F. F. Karney, Contrib. Plasma Phys. 34 (1994) 392.

[8] T. Fujimoto, J. Quant. Spectrosc. Radiat. Transfer 21 (1979) 439.

[9] M. Goto, J. Quant. Spectrosc. Radiat. Transfer 76 (2003) 331.

[10] P. T. Greenland, Proc. R. Soc. Lond. A 457 (2001) 1821.

[11] D. R. Bates et al., Proc. Roy. Soc. Lond. A 267 (1962) 297.

[12] L. C. Johnson, E. Hinnov, J. Quant. Spectrosc. Radiat. Transfer 13 (1973) 333.

[13] J. R. Myra et al., Bull. Am. Phys. Soc. 50 (2005) 323.

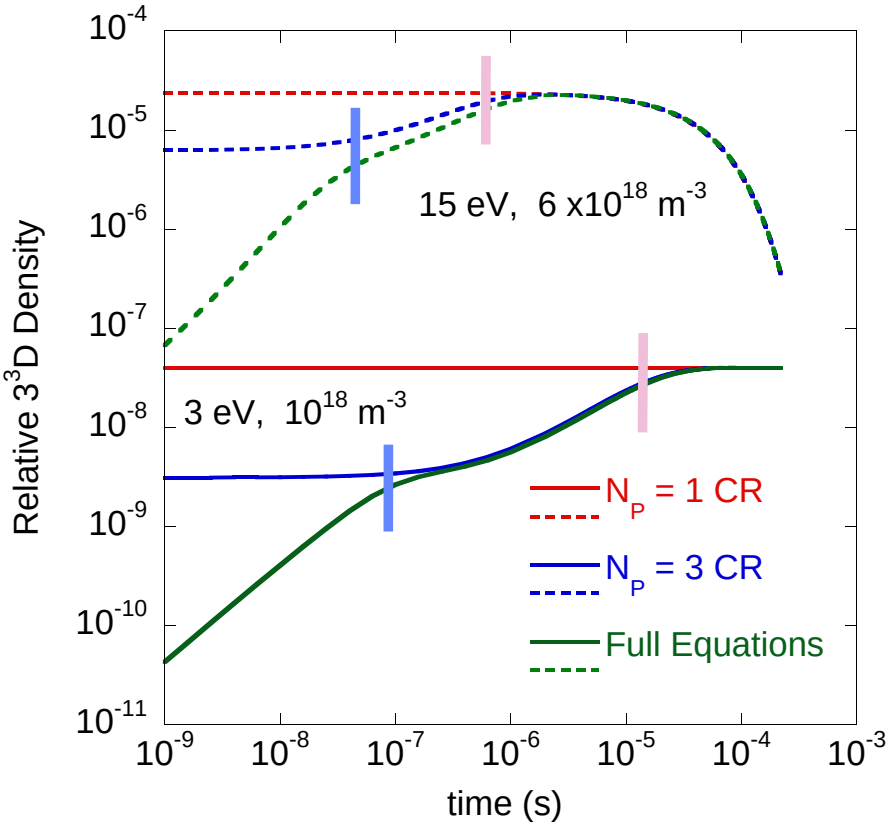

Figure 1. Evolution of the 3^3D density starting with unit ground state density. Three curves are shown for each set of plasma parameters, corresponding to the two collisional radiative models, Eqs. (3) and (4), with $N_P = 1$ and 3, and the full set of equations, Eq. (1). The values of τ_Q from Table 1 are shown as pink (blue) vertical bars for $N_P = 1$ (3).

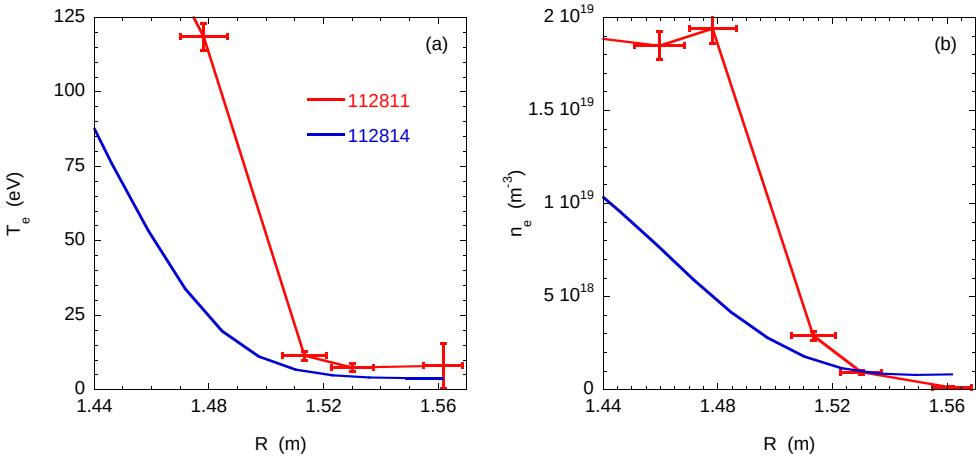

Figure 2. Thomson scattering electron temperature (a) and density (b) profiles used in DEGAS 2 simulations of shots 112811 and 112814. Since the data from 112811 are used directly, the associated error bars are also plotted. The profiles for 112814 are the average of the smoothed Thomson scattering (TS) profiles for time slices before and after the GPI time.

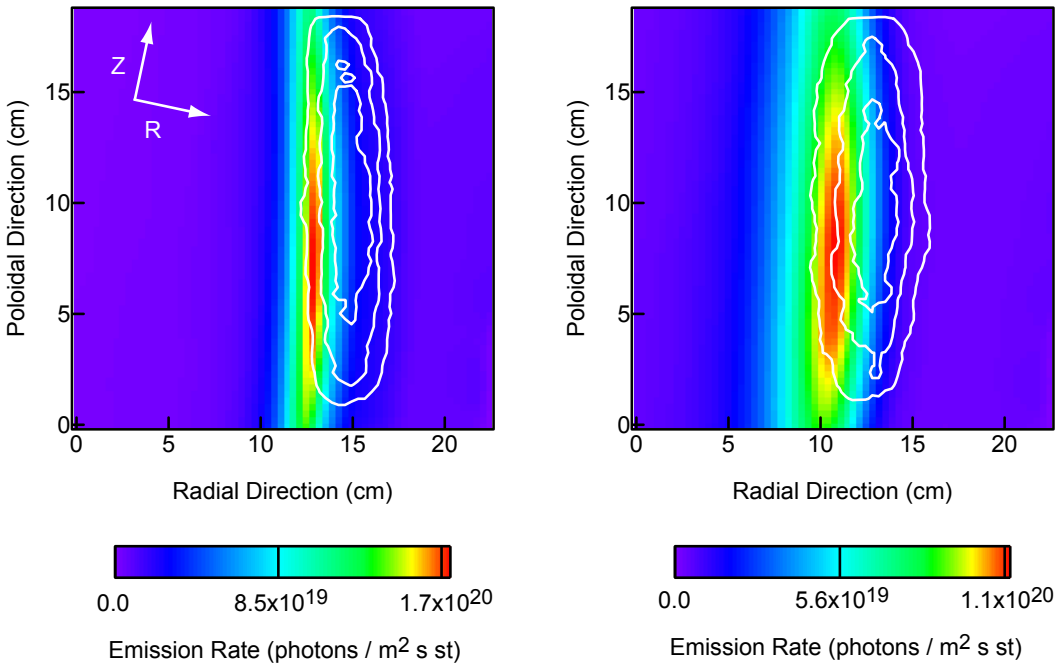

(a) (b)

Figure 3. Simulated (color images) and observed (line contours) camera data for NSTX shots 118211 (a) and 118214 (b). The experimental data are not absolutely calibrated. The simulations assume an experimentally relevant source rate of 6×10^{20} atoms / s [3]. The arrows in (a) indicate the directions of increasing major radius R and height above midplane Z.